Innovative Algorithms to Improve Long Range RTK Reliability and Availability

Liwen Dai, Dan Eslinger, Tenny Sharpe, *NavCom Technology, Inc.*

BIOGRAPHY

Liwen Dai is Advanced Navigation Algorithms Team Lead at NavCom Technology, Inc. He received a B.Sc. and M.Sc. in Geodesy in 1995 and 1998, respectively, from the Wuhan University and Ph.D. in 2002 from the University of New South Wales. His professional research interest is focused on high-precision real-time kinematic positioning, global differential GPS and GPS/INS integration.

Dan Eslinger is Manager of GPS products software at NavCom Technology, Inc. He received a B.S. in Geomatics from University of Calgary in 2000 and a Masters in Business Administration from the University of Southern California, Los Angeles, in 2006. He has a worked in various Software Engineering roles for over 6 years in Artificial Intelligence, GIS, Marine Surveying and Carrier Phase Navigation. His specializations include system design, system analysis and real-time GNSS navigation algorithms.

Tenny Sharpe is Director of Software Development at NavCom Technology, Inc. He received a B.S. in Physics from Case Institute of Technology in 1969 and an M.S. in Computer Science from the University of California, Los Angeles, in 1976. He has over 30 years' experience in the development of aerospace and industrial electronics. His specializations are software and systems design for GPS navigation systems. He has played a primary role in the development of the StarFire WADGPS.

ABSTRACT

Resolving the GPS carrier-phase integer ambiguities reliably and quickly has been a cornerstone of state-of-the-art high precision GPS positioning techniques. The challenge of doing so in real time and over long baselines is much greater due to errors introduced by the spatial de-correlation of differential atmospheric biases and orbital errors. This paper presents innovative algorithms, which have been developed to deal with these error sources and thereby significantly improve long range Real-Time Kinematic (RTK) fix reliability and availability.

The overall architecture of the new ambiguity resolution algorithm is based upon a modified LAMBDA method. The unique and innovative techniques used include; 1) an extended functional model to estimate the atmospheric biases and integration of real-time orbit corrections from WADGPS systems, 2) a modified Kalman filter with optimal detection and estimation of cycle slips and code outliers, and 3) partial search and fix strategies embedded in the Kalman filter parameter estimation. The partial search/fix techniques are used to assist in validating the integer ambiguities by excluding selected integer ambiguity values to help discriminate between the best and second best candidates. It is shown how these techniques significantly reduces the time to first RTK fix without sacrificing reliability, especially for long-range baselines and challenging signal environments.

Development of the algorithms has been completed including extensive offline testing with recorded data and hosting of the real-time version in the target GPS receiver. Both offline and real-time results are presented using extensive recorded data collected over baselines ranging up to 75 km in length. The reliability of integer ambiguity is shown to be from 99.6% to 99.99% probability of being correct. Ambiguity search times are typically one or two 1Hz epochs for baselines less than 20 km.

INTRODUCTION

High precision GPS kinematic positioning has been widely used for many surveying and navigation applications on land, at sea and in the air. The distance from the user receiver to the nearest reference receiver may range from a few kilometers to hundreds of kilometers. As the receiver separation increases, the problem of accounting for distance-dependent biases grows and, as a consequence, reliable ambiguity resolution becomes an even greater challenge. The major challenge is that the residual biases or errors after double-differencing can only be neglected for ambiguity resolution purposes when the distance between the two receivers is less than about 10km. For longer baselines, the distance-dependent errors, such as ionospheric and tropospheric delays and orbital error become significant problems.

When GPS signals are continuously tracked and no loss-of-lock occurs, the integer ambiguities resolved at the beginning of a survey can be kept for the entire GPS

kinematic positioning span. However, the GPS satellite signals may be occasionally shaded (e.g. due to buildings in "urban canyon" environments), or momentarily blocked (e.g. when the receiver passes under a bridge or through a tunnel). Generally in such cases, the integer ambiguity values are "lost" and must be re-determined. This process can take from a few tens of seconds to several minutes. In fact, the presence of significant multipath errors or unmodeled systematic biases in one or more measurements of either pseudorange or carrier phase may make it impossible with present commercial GPS RTK systems to resolve the ambiguities. As the receiver separation increases, the distance-dependent biases (e.g. orbit errors and ionospheric and tropospheric effects) grow and, as a consequence, reliable ambiguity resolution (or re-initialization) becomes an even greater challenge.

In this paper, innovative algorithms, which are suitable for running in the user receiver, are developed which significantly improve the fix reliability and availability for long-range real-time kinematic applications. They include; 1) an extended functional model to estimate the residual atmospheric biases; 2) a modified Kalman filter to deal optimally with cycle slips and/or code outlier detection, identification and estimation without the need to recompute an intermediate matrix; and 3) a partial search and fix strategy embedded within the Kalman filter parameter estimation using algorithms based upon the LAMBDA method. Residual ionosphere biases for each ambiguity pair and a relative troposphere zenith scale factor are estimated as a Gauss Markov process in the Kalman filter together with the traditional position, velocity and L1/L2 ambiguity states. Real time orbit corrections from either the StarFire network or the WAAS system could be applied in order to mitigate orbit biases for long range RTK if they are available. Based upon the float solution estimation using double difference code and carrier-phase measurements, the L1 and L2 ambiguity vector and associated variance will be translated into an L1 and wide lane (WL) state space. The partial fix strategy, which excludes different ambiguity integer values between the best and second best candidates, can be applied if the regular search results fail to satisfy the validation discrimination tests. Finally the fixed L1/WL ambiguity vector and variance-covariance matrix will be translated back into the L1/L2 ambiguity state space after the regular L1/WL search, the partial L1/WL search or even the wide lane only search successfully pass a series of validation criteria. These innovative approaches can make a significant contribution to improving RTK fix availability and reliability for long-range baselines and in other challenging environments.

MATHEMATICAL MODEL

Observable Function Model

In precise GPS positioning, double-difference (DD) carrier-phase measurements are usually formed because the differencing can cancel or mitigate many of the systematic errors which occur within the GPS measurements. As a result the DD measurements can use a simplified mathematical model. The double-difference code and carrier-phase observables at the L1 and L2 frequencies, in units of meters, can be formed as equations (1-2):

$$\nabla\Delta P_i = \nabla\Delta\rho + \nabla\Delta T + \frac{\nabla\Delta I}{f_i^2} + \varepsilon_{\nabla\Delta P_i} \quad (1)$$

$$\lambda_i \nabla\Delta\phi_i = \nabla\Delta\rho + \nabla\Delta T - \frac{\nabla\Delta I}{f_i^2} + \lambda_i \cdot \nabla\Delta N_i + \varepsilon_{\nabla\Delta\phi_i} \quad (2)$$

Where:

- subscript *i* denotes the frequency of an observable (i.e. L1/L2 and L5 in the future).
- P_i are the pseudorange observables
- ϕ_i are the carrier phase observables
- $\nabla\Delta$ denotes a double difference operation
- ρ is the geometric distance from the satellite to the receiver.
- $\nabla\Delta T$ is the residual differential tropospheric bias, which is classically represented as a function of the residual zenith tropospheric delay and a mapping function with respect to the elevation angle
- $\nabla\Delta I$ is the double differential ionospheric bias, which is estimated for each satellite pair. λ_i and f_i are the wavelength and frequency of the i[th] carrier frequency. $\nabla\Delta N_i$ is the DD integer ambiguity for the i[th] carrier frequency.
- $\varepsilon_{\nabla\Delta P_i}$ and $\varepsilon_{\nabla\Delta\phi_i}$ represent pseudorange and carrier phase residuals, including random measurement noise within the receivers and un-modeled systematic errors, such as multipath, orbit prediction errors

Linearization of the double differenced carrier phase and pseudorange observables can be represented by the following system of equation (3):

$$V = HX - Z \quad (3)$$

where V is the post-fit residuals, Z is the pre-fit residuals and H is the design matrix. X is the estimated state vector including the three baseline components, residual ionospheric and tropospheric biases, and dual or triple frequency ambiguities. These states will be discussed in detail in the next section.

Kalman Filter System Design

If the Kalman filter estimates after k-1 epochs are assumed to be $\hat{x}_{k-1}^{+}$ with variance P_{k-1}^{+}, the predicted state vector at the epoch k can be derived by the state Equations (4-5) based on the physical relation

$$\hat{X}_k^- = \Phi_{k-1,k} x_{k-1}^+ \tag{4}$$

$$P_k^- = \Phi_{k-1,k} P_{k-1}^+ \Phi_{k-1,k}^T + W_k \tag{5}$$

where $\hat{X}_k^-$ represents the unknown vector, also known as the state vector at epoch k. $\Phi_{k,k-1}$ is the matrix that relates X_{k-1} to X_k, called the transition matrix. W_k is the diagonal matrix whose elements are white sequences. The updated state and variance-covariance matrices using the measurement vector at epoch k (observation equation) can be derived as equations (6-8):

$$\hat{X}_k^+ = \hat{X}_k^- + KZ \tag{6}$$

$$P_k^+ = (I - KH)P_k^- \tag{7}$$

$$K = P_k^- H\left(HP_k^- H + R\right)^{-1} \tag{8}$$

Where K maps the pre-fix residuals into the solution and is called the gain matrix of the Kalman filter, R is variance-covariance of the observables, and I is the identity matrix. Substituting equation (6) into equation (3) yields the following:

$$V = -(I - HK)Z = -SZ \tag{9}$$

Where S is used to map the pre-fix residuals into post-fix residuals.

For the GPS RTK system the states shown in Table 1 have been implemented in the Kalman filter. In the future, L5 DD ambiguity states can be added to the Kalman filter state vector to handle the new GPS signals. The following section discusses the details of the Kalman filter design. It should be mentioned that only three position states are essential. Velocity and acceleration states are optional and can be enabled for those applications which require them.

State in Kalman Filter	Dimension	Comments
Position XYZ	3	Essential
Velocity XYZ	3	Optional
Acceleration XYZ	3	Optional
Residual troposphere	1	Optional
Residual DD ionosphere	N-1	Optional
L1 DD ambiguity	N-1	Optional
L2 DD ambiguity	N-1	Optional

Table 1 Kalman Filter State Design, N is the number of satellites used

Position, Velocity and Acceleration States

When the observer is nearly stationary, such as a buoy drifting at sea, or deformation monitoring of structures, the position can be modeled as a random-walk process. In this case three coordinate parameters are enough in the Kalman state vector. The transition matrix and dynamic noise based upon the random-walk model are given in equations (10) and (11).

$$\phi_{k,k-1} = e^{F(t_k - t_{k-1})} = 1 \tag{10}$$

$$Q_k = \sigma_p^2 (t_k - t_{k-1}) \tag{11}$$

In this position only model, σ_p^2 characterizes the position dynamics. When the rover receiver is not stationary but moving with a near constant velocity, the velocity is not white noise but a random-walk process. In this case, three coordinate parameters and three velocity parameters must be included in the Kalman state vector. The transition matrix and dynamic noise are then based upon an integrated random walk model.

$$\phi_{k,k-1} = \begin{bmatrix} 1 & (t_k - t_{k-1}) \\ 0 & 1 \end{bmatrix} \tag{12}$$

$$Q_k = \sigma_V^2 \begin{bmatrix} \frac{(t_k - t_{k-1})^3}{3} & \frac{(t_k - t_{k-1})^2}{2} \\ \frac{(t_k - t_{k-1})^2}{2} & (t_k - t_{k-1}) \end{bmatrix} \tag{13}$$

in this position-velocity model, σ_V^2 characterizes the velocity dynamics. It is not surprising that the position-velocity model also becomes inadequate for cases where the near-constant velocity assumption does not hold, that is, in the presence of significant accelerations. In order to accommodate acceleration, it is appropriate to add another degree of freedom for each position state. The result is a position-velocity-acceleration model for which a Gauss-Markov process is an appropriate model of the acceleration.

Assume the state vector includes position and velocity and acceleration. The rate of change of acceleration is then modeled as noise.

$$\phi_{k,k-1} = \begin{bmatrix} 1 & (t_k - t_{k-1}) & \frac{(t_k - t_{k-1})^2}{2} \\ 0 & 1 & (t_k - t_{k-1}) \\ 0 & 0 & 1 \end{bmatrix} \tag{14}$$

The dynamic model can be written as:

$$Q_k = \sigma_A^2 \begin{bmatrix} \frac{(t_k - t_{k-1})^6}{36} & \frac{(t_k - t_{k-1})^5}{12} & \frac{(t_k - t_{k-1})^4}{6} \\ \frac{(t_k - t_{k-1})^5}{12} & \frac{(t_k - t_{k-1})^4}{4} & \frac{(t_k - t_{k-1})^3}{2} \\ \frac{(t_k - t_{k-1})^4}{6} & \frac{(t_k - t_{k-1})^3}{2} & (t_k - t_{k-1})^2 \end{bmatrix} \quad (15)$$

where σ_A^2 characterizes the acceleration dynamics.

The determination of the spectral amplitude for the position random process is a best "guess" based on the expected vehicle dynamics. In many vehicular applications, the random perturbations are greater in the horizontal plane than in the vertical, this can be accommodated by selecting a value of spectral amplitude that is smaller for the altitude coordinate than for the two horizontal coordinates.

Differential Troposphere Delay State

GPS satellite signals are refracted by the lower neutral part of the earth's atmosphere extending from zero to 16 km, which is known as the troposphere and which is composed of dry gases and water vapor. The troposphere is a non-dispersive medium and therefore the refraction here does not depend on the GNSS signal frequencies. The magnitude of the tropospheric error depends upon the satellite elevation angle. It is about 2.3 m at the zenith and over 25 m for an elevation of 5 degrees. The troposphere error can be mitigated using different models such as the UNB, Hopfield or Saastamoinen models. The dry component can be modeled with high accuracy but the wet component cannot. After applying a model, the differential troposphere error, mostly the wet component, varies typically from 0.2 to 0.4 parts per million (ppm). The residual tropospheric bias is classically represented using a value for the zenith delay together with a mapping function to obtain the delay at specific satellite elevation angles. The spatial and temporal characteristics of the residual tropospheric delay, which is mostly due to the water vapor fluctuation in the atmosphere, can be characterized by probabilistic laws or statistical models. The effects of the troposphere on radio wave propagation can then be predicted over varying spatial dimensions and temporal scales by a specific probability density function or stochastically in terms of the spatial and temporal correlation of the fluctuations. In general, the residual tropospheric delay can be treated as a first-order Gauss-Markov process.

The variations of the atmospheric conditions are handled with a scaling factor for the zenith delay. After correcting the troposphere delay with the model, the "relative tropospheric zenith delay" (RTZD) can be approximately represented, as shown in equation (16), as a function of the residual zenith tropospheric delay and an elevation angle mapping function:

$$RTZD = T_{kl}^{pq} / [MF(\varepsilon^p) - MF(\varepsilon^q)] \quad (16)$$

where ε^p and ε^q are the average elevation angles of the two receivers for satellites p and q respectively. Independent of the elevation of a satellite at the base station, the RTZD is scaled by the mapping function for the elevation angle of the rover location. Obviously, this is a simplifying approximation. Empirically, the residual zenith tropospheric delay can be modeled as a first-order Gauss-Markov process. The transition matrix and dynamic model are then derived as:

$$\phi_{k,k-1} = e^{-\beta_{trop}(t_k - t_{k-1})} \quad (17)$$

$$Q_k = \frac{\sigma_{trop}^2}{2\beta_{trop}}(1 - e^{-2\beta_{trop}(t_k - t_{k-1})}) \quad (18)$$

where $1/\beta_{trop}$ is the correlation time of the troposphereric wet component and σ_{trop}^2 represents the variation of the wet component. Both are typically functions of the baseline length and perhaps the height difference as well.

Differential Ionosphere States

The ionosphere is that region of the earth's atmosphere in which ionizing radiation causes electrons to exist in sufficient quantities to affect the propagation of radio waves. The height at which the ionosphere starts is about 50 km and stretches to heights of 1000 km or more. The ionosphere is a dispersive medium for radio waves, that is, its refractive index is a function of the frequency. One characteristics of the ionosphere is that it advances the carrier phase but delays pseudorange observations. The magnitude of the ionospheric error varies according to the level of ionizing radiation, which is strongly dependent upon the level of solar radiation activity. Thus it varies between daytime and nighttime and from one season to another. Diurnally, the ionospheric error usually reaches a peak at about 14:00 local time and drops to a minimum just before sunrise. Under extreme conditions, the ionospheric error can reach 15 m in the zenith direction and more than 200 m at elevations near the horizon. . The ionosphere is the largest error source for differential processing and varies from about one part per million (ppm) of the baseline length during low ionospheric periods at mid-latitudes to greater than 10 ppm at low geomagnetic latitudes during midday. The parameters of an empirical model to approximate the ionospheric delay are broadcast by GPS satellites in real-time. These parameters can be used to partially compensate for the effects of the ionosphere delay. It is claimed that this model can provide at least a 50% reduction in the single-frequency user's RMS position error arising from the

ionosphere propagation effects. The model has also been widely used in high-precision carrier phase–based RTK applications to reduce the sensitivity to the baseline length dependence..

The residual ionosphere delay, after applying the broadcast model and differencing the measurements with the corresponding reference site measurements, can be included as an element in the state vector to be estimated in the Kalman filter. Empirically, the residual delay can be modeled as a first order Gauss-Markov process. The transition matrix $\phi_{k-1,k}$ and dynamic model Q_k can be expressed as:

$$\phi_{k-1,k} = e^{-\beta_{ion}(t_k - t_{k-1})} \tag{19}$$

$$Q_k = \frac{\sigma_{sion}^2}{2\beta_{ion}}(1 - e^{-2\beta_{ion}(t_k - t_{k-1})}) \tag{20}$$

$$\sigma_{sion} = \frac{\sigma_{vion} \times L}{\sqrt{1 - \left(\frac{R}{R+H}\cos(E)\right)^2}} \tag{21}$$

where $1/\beta_{ion}$ is the correlation time of the differential ionosphere bias, which typically varies between 30 to 300 seconds. σ_{sion} and σ_{vion} represent the typical variation of the differential slant and vertical ionosphere biases respectively. σ_{vion} which is a function of the local time and the ionosphere activity level, will typically vary between 0.5 and 2 ppm. L represents the baseline length between the base receiver and rover site. E is satellite elevation. The height of the ionospheric layer, H, is assumed to be 350 km and the radius of the earth, R, used in the model, is 6371km.

It should be noted that unlike the residual tropospheric bias, the residual ionosphere parameters are estimated for each satellites other than the reference satellite. The ionospheric correction from global or regional ionosphere models such as WAAS can be considered as virtual measurements and added into the Kalman filter estimation. However, the accuracy obtained from either the broadcast and WAAS models is not good enough to estimate carrier-phase integer ambiguities. This is because the models cover a large region of the ionosphere and can only represent the large-scale structure of the ionospheric electron content, i.e. they cannot reproduce the small-scale or medium-scale structure of the ionospheric electron content.

It should be also mentioned that over the past few years, the concept of using reference station networks for real-time kinematic GPS positioning has been promoted strongly by some academic institutions and by some GPS manufactures. These networks implementations generate 'correction terms' for the atmospheric biases and orbit errors from measurements across the network. These corrections can be used to mitigate the distance dependent errors. However, network RTK performance still significantly depends upon the linearity characteristics of the errors. This means that non-linear distant dependent errors remain and are not cancelled in the standard network RTK implementations. The improved modeling of the residual ionosphere can increase the ambiguity fixing performance and reliability; and can reduce the time to first RTK fix for both long range and network RTK.

Satellite Orbital Error Mitigation from WADGPS

Satellite orbital errors results from inaccuracies in the orbital information transmitted from the GPS satellites. These inaccuracies are due to the predicted nature of the broadcast ephemeris. The broadcast navigation message includes Keplerian orbital elements and time derivatives for these elements. It is generated using the measurements from a limited number of GPS monitor stations and is typically updated only once every two hours. Tests have shown that the orbit error is generally between 2 and 5 meters. The orbital error is generally the largest error source for long range RTK ambiguity resolution after the troposphere and ionosphere biases are estimated in the Kalman filter. Several differential GPS systems have become available which supply measurements or measurement corrections which can be used in a navigation receiver to obtain navigation results in the 10 centimeter range after the carrier-phase floating ambiguities have been determined to sufficient accuracy. These systems are of several types. The High Accuracy Nationwide Differential GPS System (HA-ND GPS) being developed cooperatively by several U.S. government organizations uses ground based reference sites. This system transmits the corrections to the user using Coast Guard beacons which can reach users at ranges of a few hundred kilometers. John Deere has developed the StarFire™ system which transmits corrections via communication satellites with both a regional wide area correction data stream and a global DGPS correction data stream. The global orbital correction stream can be used to mitigate orbital errors in long range carrier-phase differential applications. It could be of significant benefit for long range RTK ambiguity resolution.

Ambiguity States

In theory, the ambiguities are constant. However, the floating ambiguities which are estimated in the Kalman filter can contain multipath errors and other un-modeled systematic biases such as orbit and residual tropospheric and ionospheric biases remaining after their estimation in the filter. Based on these considerations, the ambiguities

before being fixed can be modeled as a random walk with very small dynamics as shown in equations (22-23)

$$\phi_{k-1,k} = 1 \tag{22}$$

$$Q_k = \delta_{amb}^2 (t_k - t_{k-1}) \tag{23}$$

where δ_{amb} is small a small dynamic noise, e.g. such as 0.001 cycle. Once the integer ambiguities are fixed, they are modeled as constants and the corresponding dynamic noise is set to zero. The small dynamic noise is very helpful in resolving some issues which can cause a long time for the ambiguities to be resolved. For example, in some special cases bad data from excessive multipath at the beginning can result in a very long time to the first fix. It can also take significant time regain a fix when the user receiver moves from a severe shading environment to the open sky. On the other hand, the ambiguities typically can be fixed in single epoch and a tiny dynamic noise does not adversely impact the time to first fix in the normal situation.

As discussed above, the differential ionospheric and tropospheric biases are modeled as first order Gauss Markov processes. When this is done, the computational efficiency becomes a critical issue, especially for real time embedded receivers. It should be noted that a significant amount of optimization can be realized because the sparse design matrix, H, contains many zero elements. Another challenging issue for a large Kalman filter embedded within a user receiver, is how to efficiently deal with outliers and cycle slips in the GPS code and carrier-phase measurements. In the next section, a method for detecting, identifying and estimating the presence of cycle slips and code outliers within a modified Kalman filter and in an optimal fashion is considered.

MODIFIED KALMAN FILTER FOR SLIP AND OUTLIER ESTIMATION

In the presence of outliers or cycle slips, the observation equation (3) can be extended to estimate cycle slips or outliers. This extension is presented in equation (24).

$$V = HX + GY - Z \tag{24}$$

where Y is the estimated cycle slip or outlier vector with size p and G is an n x p coefficient matrix. The parameter p is the size of the estimated slips or outliers. The elements of the G matrix are zero for all good measurements or one for measurements with outliers. For example, in the special case where there is a slip or outlier in the measurement from the reference satellite, all n x 1 elements of G matrix are set to one.

It should be noted that not only can the measurements contain outliers, but also the Kalman filter states and the associated variance-covariance elements can be significantly biased due to incorrect dynamic assumption. The Kalman filter can be extended to handle these situations. However, in this paper the focus is on measurements outliers and cycle slips only.

Because the predicted states and associated variance can be considered as virtual measurements with expectation, X_k^- , and variance-covariance, P_k^- , they can be written in a generic Least-Square form as equation (25).

$$V_X = X + X_k^- - X_k^- \tag{25}$$

Equations (24-25) can be grouped into the following:

$$\overline{V} = \begin{pmatrix} V \\ V_X \end{pmatrix} = \begin{pmatrix} H & G \\ I & 0 \end{pmatrix} \overline{X} - \begin{pmatrix} Z \\ 0 \end{pmatrix} \tag{26}$$

where $\overline{X} = \begin{pmatrix} X \\ Y \end{pmatrix}$ and the corresponding variance-covariance matrix for the unknown parameters estimation can be given as equation (27)

$$\overline{R} = \begin{pmatrix} R & 0 \\ 0 & P_k^- \end{pmatrix} \tag{27}$$

The bias-free least-squares solution to equations (26-27) considers the effect of outliers and cycle slips and is designed to minimize $\overline{V}^T \overline{R}^{-1} \overline{V}$.

$$\begin{aligned} \frac{\partial\left(\overline{V}^T \overline{R}^{-1} \overline{V}\right)}{\partial \overline{X}} &= 2\overline{V}^T \overline{R}^{-1} \frac{\partial \overline{V}}{\partial \overline{X}} \\ &= 2\overline{V}^T \overline{R}^{-1} \begin{pmatrix} H & G \\ E & 0 \end{pmatrix} = 0 \end{aligned} \tag{28}$$

Substituting Equation (26) into Equation (28) yields the following:

$$\begin{pmatrix} H^T R^{-1} H + \left(P_k^-\right)^{-1} & H^T R^{-1} G \\ G^T R^{-1} H & G^T R^{-1} G \end{pmatrix} \begin{pmatrix} X \\ Y \end{pmatrix} = \begin{pmatrix} H^T R^{-1} Z \\ G^T R^{-1} Z \end{pmatrix} \tag{29}$$

The first part of Equation (29) can be represented as

$$\begin{aligned} X &= \left(H^T R^{-1} H + \left(P_k^-\right)^{-1}\right)^{-1} \left(H^T R^{-1} Z - H^T R^{-1} G Y\right) \\ &= \left(H^T R^{-1} H + \left(P_k^-\right)^{-1}\right)^{-1} H^T R^{-1} \left(Z - GY\right) \\ &= P_k^- H^T \left(R + H P_k^- H^T\right)^{-1} \left(Z - GY\right) \\ &= K\left(Z - GY\right) \end{aligned} \tag{30}$$

By substituting equation (30) into the second part of equation (29), outliers and cycle slips represented by the vector **Y** can be estimated through:

$$G^T R^{-1} \left(I - HK\right) G Y = G^T R^{-1} \left(I - HK\right) Z$$

$$Y = \left(G^T R^{-1} SG\right)^{-1} G^T R^{-1} SZ$$
$$= \left(G^T UG\right)^{-1} G^T UZ \quad \text{where } U = R^{-1} S \tag{31}$$

The variance for the outliers or cycle slip vector, P_Y, can be estimated as:

$$P_Y = \left(G^T UG\right)^{-1} \tag{32}$$

Equations (31-32) clearly illustrate that the outliers or slips Y vector and variance-covariance matrix can be estimated using the gain K, the residual mapping matrix, S, and the weight matrix R^{-1}, after the outliers are identified in matrix G. It should be mentioned that the matrices K, S, and R^{-1}, do not need to be recomputed during the iteration over outlier and cycle-slip detection.

After adjusting for outliers or cycle slips, the Kalman filter state and variance-covariance matrix can be estimated using:

$$X_k^+ = X_k^- + X = X_k^- + K\left(Z - GY\right) \tag{33}$$

$$P_k^+ = P_k^- - KHP_k^- + KGP_Y G^T K^T \tag{34}$$

Equations (33-35) indicate that the final KF states and variance-covariance can be recomputed based on the Y, and P_Y estimation and the K, G matrices.

The post-fit residual for carrier-phase and code measurements can be derived after the outlier or cycle slips are estimated.

$$V = HX + GY - Z$$
$$= HK\left(Z - GY\right) - \left(Z - GY\right)$$
$$= -\left(E - HK\right)\left(Z - GY\right) \tag{35}$$
$$= -S\left(Z - GY\right)$$

Though the above derivation is based on a classical Kalman filter, similar equation can be derived for the least–square method.

Both the carrier-phase and pseudorange measurements are used to estimate the real-valued state vector, including user receiver coordinates, ambiguities, residual tropospheric and ionospheric biases, and their variance-covariance matrix. Reliable results at this step are dependent upon the appropriateness of the stochastic model of the measurements with respect to the functional model. The following rejection region in equation (36) should be employed in order to check the fidelity of the stochastic and functional models:

$$V^T R^{-1} V > \sigma_0^2 \cdot \xi_{\chi^2_{ndf};1-\alpha} \tag{36}$$

where $V^T R^{-1} V$ is the quadratic form of the post-fit residuals, $\xi_{\chi^2_{ndf};1-\alpha}$ is the upper boundaries of the $1-\alpha$ confidence interval for the χ^2-distribution statistic with the number of degrees of freedom. This test is used to test the pseudorange and carrier-phase observation quality. If the $V^T R^{-1} V$ is rejected by equation (36), the outlier and cycle slip detection procedure should be applied because outliers or cycle slips may exist in the measurements. Such outliers can be caused by multipath or system biases or a stochastic model that does not reflect the actual accuracy of the observation.

Any measurement error, including outliers, affects the post-fit residuals through the matrix S in the equation (9 or 35). The correlation coefficient between column vectors of the reliability matrix S and the residual vector is considered to be critical information. Such a correlation can show the presence of a true error in the measurements which is reflected in the residuals (Dai, 1999, Hatch, 2003). The measurement(s) related to the most significant correlation coefficient(s) should be suspected of having been contaminated by outliers or cycle slips. The measurement with the largest correlation coefficient can be identified and excluded for each of the iterations. Hence, multiple outliers can be located through an iterative procedure. After the outliers have been located, they can be estimated using the equations (31-32). The bias-free Kalman filter solution can be derived from equations (33-34). The advantage of this approach is computational efficiency and no need to recompute the intermediate matrices such as the gain matrix. There is significant benefit from the proposed innovative algorithm, especially for a large Kalman filter like that proposed herein, when it is embedded within a receiver with limited computational resources.

PARTIAL SEARCH TECHNIQUE

When the integer ambiguities are resolved improperly, it can be very difficult to identify which ambiguity is incorrect. But if the ambiguities are resolved improperly, it is clear that one or more of the estimated floating ambiguities contains a significant bias. For the ambiguity resolution, a minimum of five satellites is required. When six or more satellites are observed, some of the ambiguities can be arbitrarily removed from the search process. By computing all combinations of five or more satellites it may be possible to isolate one or more of the floating ambiguities with significant biases and a successful ambiguity resolution may result. This procedure could be implemented in the software by eliminating one (or more) satellites (keeping at least five). If the ambiguity resolution fails, the procedure can be repeated until the resolution is successful. If all possible sets of five or more satellites have been tested and the ambiguity test still fails, the ambiguity resolution procedure has failed at least until more measurement data is collected. The above procedure for searching through subsets significantly increases the ambiguity resolution success rate. However, these combined search processes

take significant time to compute and it is generally impossible to search all combinations in the software embedded within the GPS receivers because of limited processing resources.

The following innovative partial search technique is proposed. After the double-difference measurements from both frequencies are processed, the floating ambiguity vector and the associated variance-covariance can be obtained via equations (6 & 7) from the Kalman filter estimation. Although the L1 and L2 floating ambiguities are the parameters estimated, the ambiguity pairs to be searched in the LAMBDA method, may be different. In this paper, $\hat{N}_1$ and the wide lane $\hat{N}_{(1,-1)}$ are chosen for the search process. They are formed from the original L1 and L2 float ambiguity vector of equation (2) using the following equation:

$$\begin{pmatrix} \hat{N}_1 \\ \hat{N}_{(1,-1)} \end{pmatrix} = \begin{pmatrix} 1 & 0 \\ 1 & -1 \end{pmatrix} \begin{pmatrix} \hat{N}_1 \\ \hat{N}_2 \end{pmatrix} \quad (37)$$

Based on equations (8-9), the variance-covariance matrix of $\hat{N}_1$ and the wide lane $\hat{N}_{(1,-1)}$ is obtained as follows:

$$\mathrm{Q}_{\hat{\mathrm{N}}_1,\hat{N}_{(1,-1)}} = \begin{pmatrix} 1 & 0 \\ 1 & -1 \end{pmatrix} \begin{pmatrix} Q_{N_1} & Q_{N_1N_2} \\ Q_{N_2N_1} & Q_{N_2} \end{pmatrix} \begin{pmatrix} 1 & 1 \\ 0 & -1 \end{pmatrix} \quad (38)$$

The best integer vector candidate and second best integer vector can be found during the Lambda search process. If the ambiguity validation discrimination tests have been passed, the best integer ambiguity vector will be accepted as the correct ambiguity set to produce the fixed solution. If no ambiguity pairs are excluded from the search process, the search results of $\hat{N}_1, \hat{N}_{(1,-1)}$ and $\hat{N}_1, \hat{N}_2$ are identical. However, they will differ if some ambiguities are excluded from the search process. It is well known that the wide-lane ambiguity is easy to resolve due to the longer, 0.86 cm, wavelength. The common practice is to first to fix the wide lane ambiguity followed by the L1 ambiguity. The partial fix procedure is applied when the combination fix of $\hat{N}_1, \hat{N}_{(1,-1)}$ fails to pass the discrimination test criterion. The partial search technique is to exclude those satellites whose integer ambiguities are different between the best candidate set and the second best candidate set from the LAMBDA search process. In most cases, one or more $\hat{N}_1$ ambiguities are excluded in the partial search, but all of the wide lane ambiguities remain in the partial search. This partial search process can be repeatedly applied until the minimum of five ambiguities no longer remain to be searched. If the partial $\hat{N}_1, \hat{N}_{(1,-1)}$ search fails, only $\hat{N}_{(1,-1)}$ or partial $\hat{N}_{(1,-1)}$ ambiguities can be used in the LAMBDA search process. It is obvious that the partial fix procedure can be used to increase the fix availability, especially in long range applications where biases are more common.

If the fix or partial fix successfully passes the ambiguity discrimination test, equations (39-40) can be used to recover the original L1 and L2 ambiguities states and the variance-covariance in the Kalman filter.

$$\begin{pmatrix} \hat{N}_1 \\ \hat{N}_2 \end{pmatrix} = \begin{pmatrix} 1 & 0 \\ 1 & -1 \end{pmatrix} \begin{pmatrix} \hat{X}_{N_1} \\ \hat{X}_{N_{(1,-1)}} \end{pmatrix} \quad (39)$$

$$\mathrm{Q}_{\hat{\mathrm{N}}_1,\hat{N}_2} = \begin{pmatrix} 1 & 0 \\ 1 & -1 \end{pmatrix} \begin{pmatrix} Q_{N_1} & Q_{N_1N_{(1,-1)}} \\ Q_{N_{(1,-1)}N_1} & Q_{N_{(-1,1)}} \end{pmatrix} \begin{pmatrix} 1 & 1 \\ 0 & -1 \end{pmatrix} \quad (40)$$

Note, if $\hat{N}_1$ is floating but $\hat{N}_{(1,-1)}$ is fixed, the fractional part of $\hat{N}_1$ and $\hat{N}_2$ are exactly the same, and the variance of Q_{N_1}, Q_{N_2} and covariance $\mathrm{Q}_{N_1N_2}$ are the also the same. If $\hat{N}_1$ is fixed later, the fixed value of $\hat{N}_1$ and $\hat{N}_2$ will be adjusted to an integer value and the variance and co-variance will become zero.

The proposed partial search technique has significant advantages: (1) it is a rigorous approach from a Kalman filter implementation point of view; (2) all other approaches to fix ambiguity and wide lane ambiguities, e.g. L1/L2 search and wide lane only searches, are simply special cases of the above process, and; (3) it can significantly improve RTK ambiguity resolution availability and reliability, especially for long-range applications and in other challenging environments.

TEST RESULTS

In order to evaluate the proposed three innovative algorithms, the extensive off-line post-processing tests and real time kinematic tests are conducted.

Post Processing Tests

NavCom Technology Inc. established a GPS reference network consisting of 10 receivers within the greater Los Angles area. Figure (1) illustrates the locations of the deployed GPS reference network. Each site is equipped with a dual frequency NavCom receiver and antenna. The implementation calls utilizes an intranet in order to collect the data from each of the reference network receivers at a central location.

Figure (1) Network Configuration

Twenty days of data were selected from the reference network between May and July 2006 in order to evaluate the performance of RTK algorithms described above. Data analysis focused on time-to-fix, reliability and positioning accuracy. It is important to note that no any network RTK corrections have been applied for RTK offline processing that is presented below. The test was conducted on 45 baselines with lengths up to 75km. The data was post-processed using the offline RTK software in kinematic mode, utilizing the same algorithms as hosted in the receiver firmware. An automatic system reset was used to re-initialize the whole system after fix.

Time-To-WideLane (TTWL) and Time-To-L1L2 (TTL1L2) are defined as the time, in seconds, after 5 or more satellites are tracked, until wide lane or L1L2 ambiguities are resolved respectively. Figure (2) illustrates TTWL performance over short, medium and long baselines up to 75km. The TTWL can be achieved within 1s, 1s, 7s, 53s, 135s, 232s for 4.2km, 11.5km, 24.2km, 32.3km, 47.8km and 74.4km baselines respectively, for the 95% of the time during 20-days data.

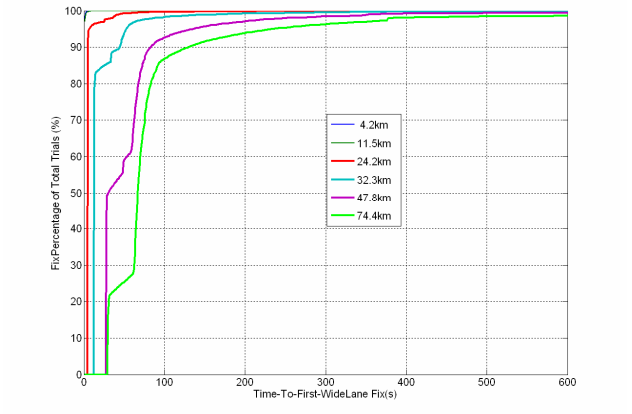

Figure (2) Time-To-WL Fix

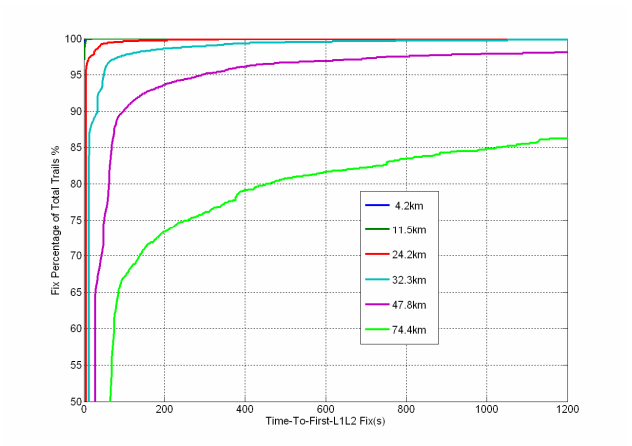

Figure (3) Time-To-First L1L2 Fix

Figure (3) illustrates TTL1L2 performance over short, medium and long baselines. The TTL1L2 can be achieved within 1s, 1s, 8s, 81s, 294s, 5096s for 4.2km, 11.5km, 24.2km, 32.3km, 47.8km and 74.4km baselines respectively, for the 95% of the time during for the sample data set previously described. It can be seen that the TTL1L2 for baseline 74.4km is significant longer.

Figure (4) illustrates the fix reliability, which refers to the ratio value between the number of correct ambiguity fixes and the number of the total ambiguity fixes. The data set used provided over 1.5 million resets for short baselines and roughly 5 thousands resets for long baselines. It can be seen that 99.99% fix reliability can be achieved for 10km or less baseline and 99.9% reliability still can be achieved for baselines up to 40km. As the baselines exceed 40km, the reliability decreases to 99.6% at a baseline of 75km. It should be noted that the ionospheric activity is relatively quiet during this test period. As a result, the RTK performance may degrade when the level of solar radiation activity increases.

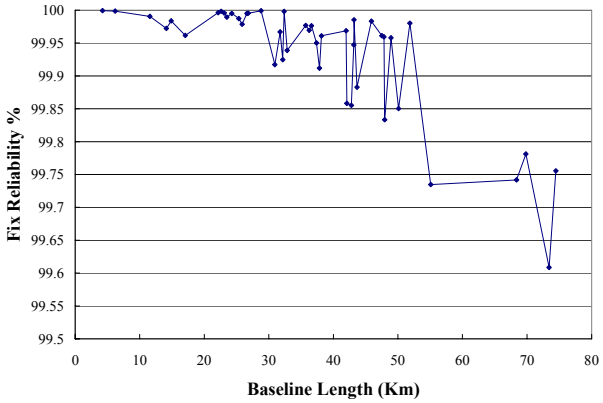

Figure (4) RTK fix reliability

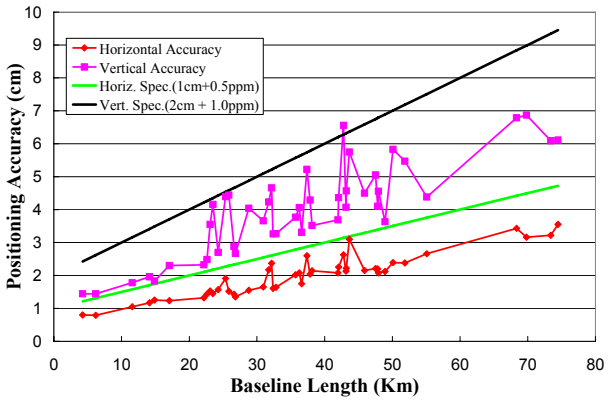

Figure (5) RTK Positioning Accuracy

GPS positioning accuracy depends on the satellite geometry, number of fixed ambiguities and residual errors from various sources, including measurement noise, multipath and other unmodeled errors. The NavCom RTK system reduces these errors by employing advanced multipath mitigation techniques and appropriate stochastic modeling including modeling atmospheric biases. Figure (5) demonstrates the horizontal and vertical accuracy over 45-baselines computed from 24 hour RTK kinematic positioning results. Figures (6) and (7) demonstrate the horizontal and vertical positioning error distribution for 4.2km, 11.5km, 24.2km, 32.3km, 47.8km and 74.4km baselines. The positioning accuracies meet the formal error specifications of 1cm + 0.5ppm in horizontal and 2cm + 1pmm in vertical.

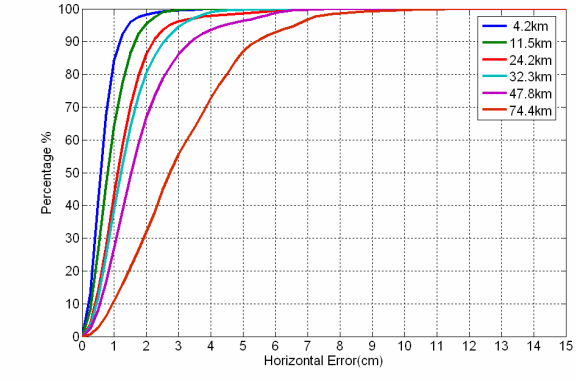

Figure (6) Horizontal positioning errors for 4.2km, 11.5km, 24.2km, 32.3km, 47.8km and 74.4km baselines

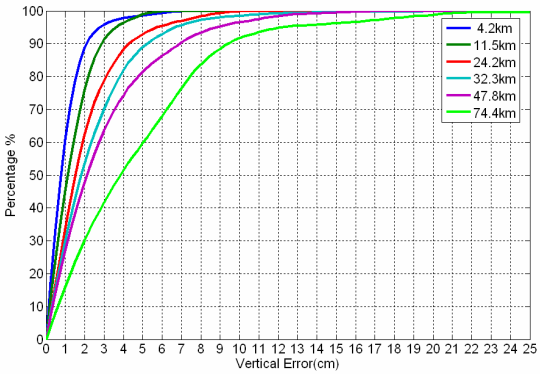

Figure (7) Vertical positioning errors for 4.2km, 11.5km, 24.2km, 32.3km, 47.8km and 74.4km baselines

Figures (8a) through (8e) demonstrate typical 24 hour RTK positioning results for various baselines including 4km, 24km, 32km, 47km and 70km respectively. These results were computed from offline RTK engine processing in truly kinematic mode without manual reset.

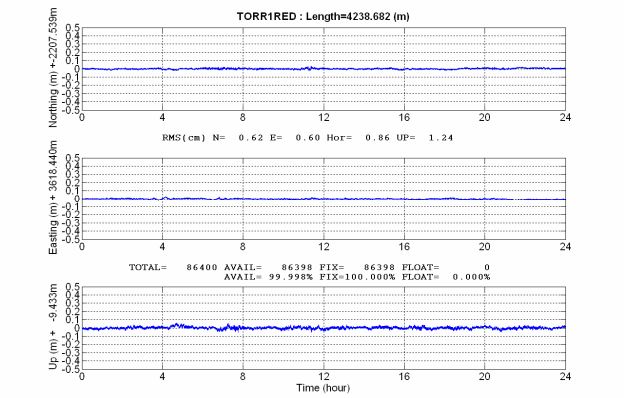

Figure (8-a) 4km short baseline RTK Positioning Results

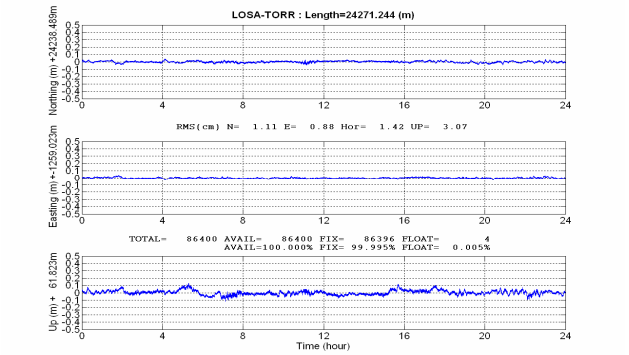

Figure (8-b) 24km RTK Positioning Results

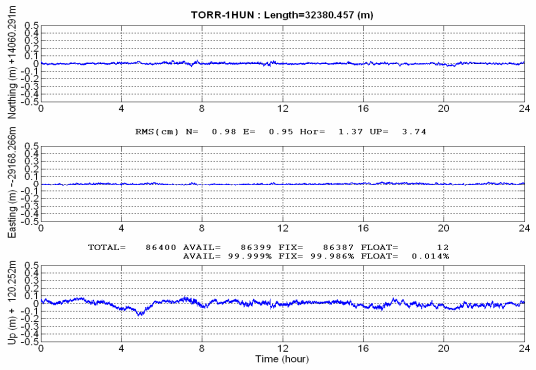

Figure (8-c) 32km RTK Positioning Results

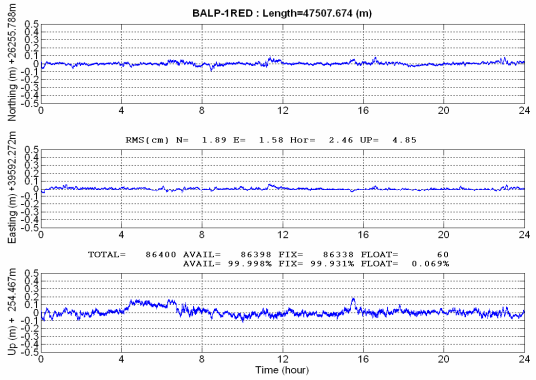

Figure (8-d) 47km RTK Positioning Results

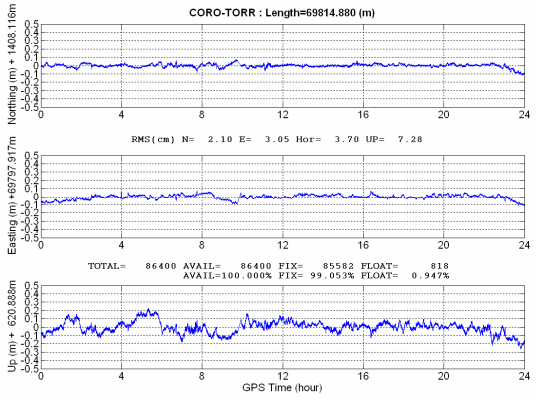

Figure (8-e) 70km RTK Positioning Results

Real Time Kinematic Results

The second is a real time kinematic experiment carried out on October 5 2006 using four dual-frequency NCT2100D rover receivers. Two reference sites (1SAN and 1ANA) were chosen as the base stations for these dynamic RTK tests. The baselines between rovers and base stations are nominally 11km and 38km respectively. The base station RTK corrections were distributed via TCP/IP internet and broadcast by two Raven radio moderns in the Torrance office and each base station correction stream was divided into two rover receivers as illustrated in Figure 9. Two GPS antenna were mounted on the top of test vehicle. The trajectory and height profile of the rover receivers during the test period are shown in Figure 10.

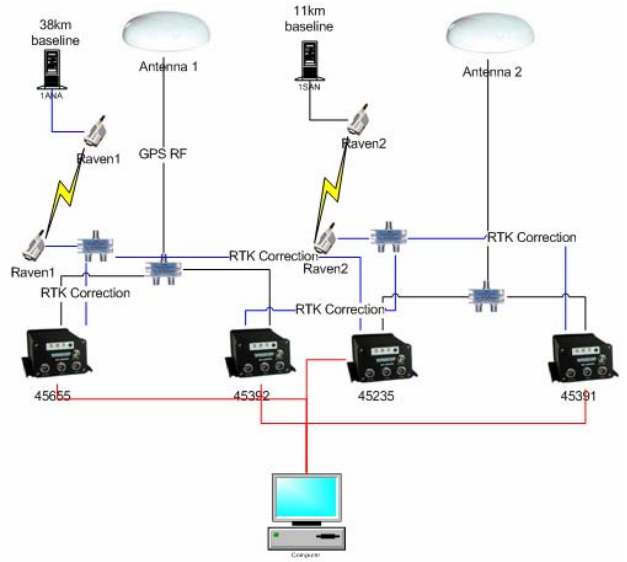

Figure (9) Configuration for the kinematic experiment.

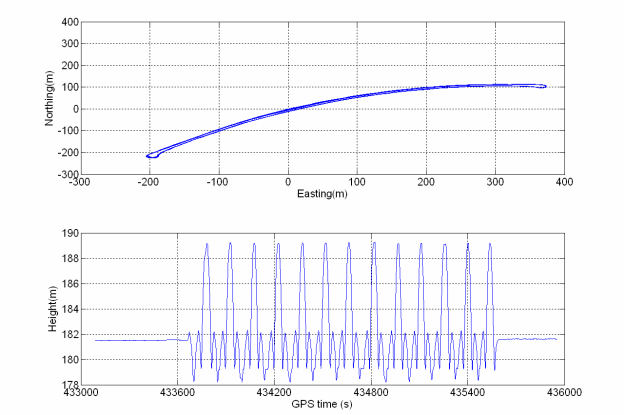

Figure (10) Trajectory of real time kinematic test.

This test configuration was used so that performance could be evaluated due to the observation that two receivers connected to the same antenna should have same positioning coordinates and there is constant distance between two different rover antennas. These conditions can be used as a mutual check on whether the derived positioning results are correct. After the first 10 minutes in static mode, the vehicle traveled around local streets under open sky view, and completed the experiment in static mode again for 5 minutes. A total of 13 kinematic loops were completed with 1Hz data rate. A single computer was used to log all four rover raw observables and real time positioning results. The number of observed satellites and PDOP are plotted in Figure 11. During this test, there were 6-7 satellites above the 7 degree elevation navigation mask angle and PDOP values ranged from 2 to 4.

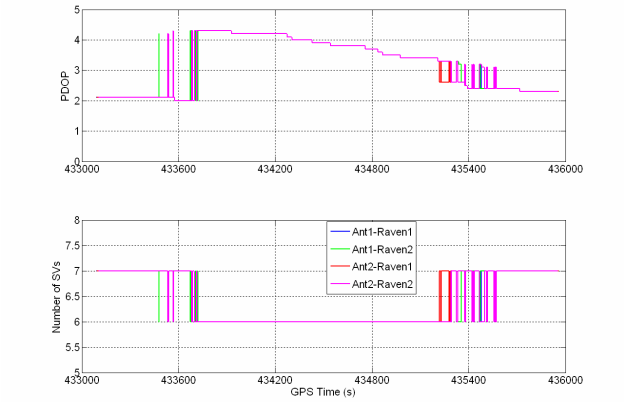

Figure (11) The number of satellites and PDOP

Figure (12) plotted the velocity during kinematic test. The horizontal speed varied from 0 to 40km/hour. Maximum vertical speed was about 1m/s.

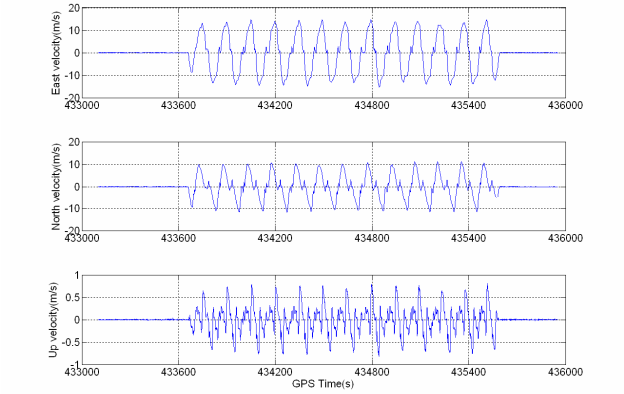

Figure (12) Velocity components.

There are two options of the base correction for RTK engine usage, so called time synchronized mode and low latency mode. Low latency mode was chosen for this test. Figure (13) gave the base corrections age. Typically 2-3s delay, sometimes, up to 6-7 due to the TCP/IP traffic and Raven modem communications delay or drops. For long range RTK applications, it is recommended that the time synchronized mode should be used to avoid the correction errors resulted from old data age. The NavCom receivers deployed a simple and very efficient algorithm for propagating the position forward in time at a high rate using the change in carrier-phase measurements at the high-rate epoch interval (R. Hatch, 2004). It is very accurate and does not limit the accuracy when used in even the highest precision RTK mode. By combining these techniques, NavCom receivers are able to provide low latency and high accuracy time synchronized RTK solutions for long baseline applications.

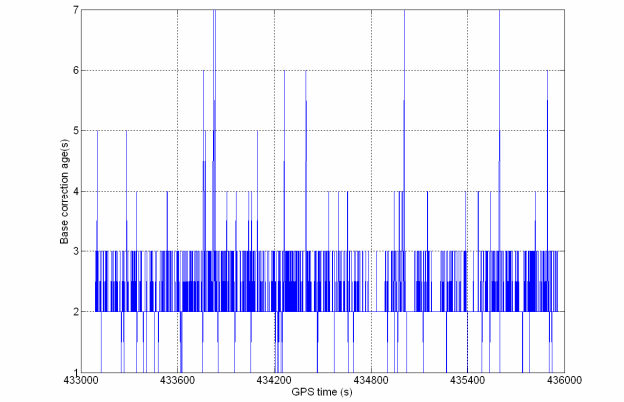

Figure (13) RTK rover correction age

Figure (14) shows the positioning difference of rovers receivers connected with the same antenna. They can used to evaluate RTK fix performance. It should be mentioned that the each receiver has different base correction. Since it is very unlikely that same amount of poisoning bias will be observed from both receivers due to a wrong fix, the results indicate that the dynamic performance is on par with the static performance. Figure (14) clearly demonstrates that the accuracy against the zero for the differences of north and east component is less than 2cm and vertical about 5cm. It is again reinforces that the positioning accuracy meets the product positioning accuracy specifications at 1cm + 0.5ppm in horizontal and 2cm + 1pmm in vertical.

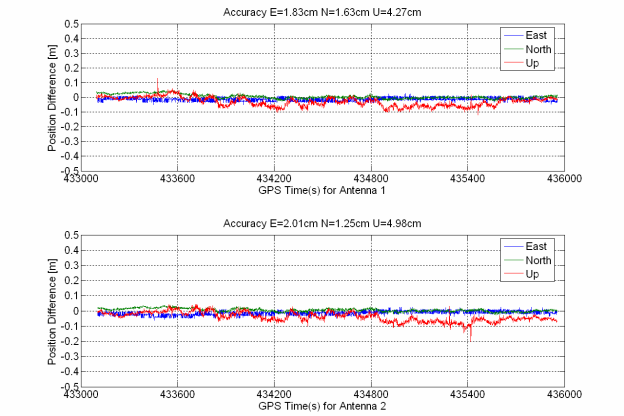

Figure (14) Position difference from the same antenna

Figure (15) plotted the distance difference between the different antennas. It can be seen that three components changed during kinematic test period, but the distance did not. The constant distance (nominally 92cm) between the two antennas is used to verify that the kinematic positioning results are correct. Once again, the results demonstrate excellent real time performance.

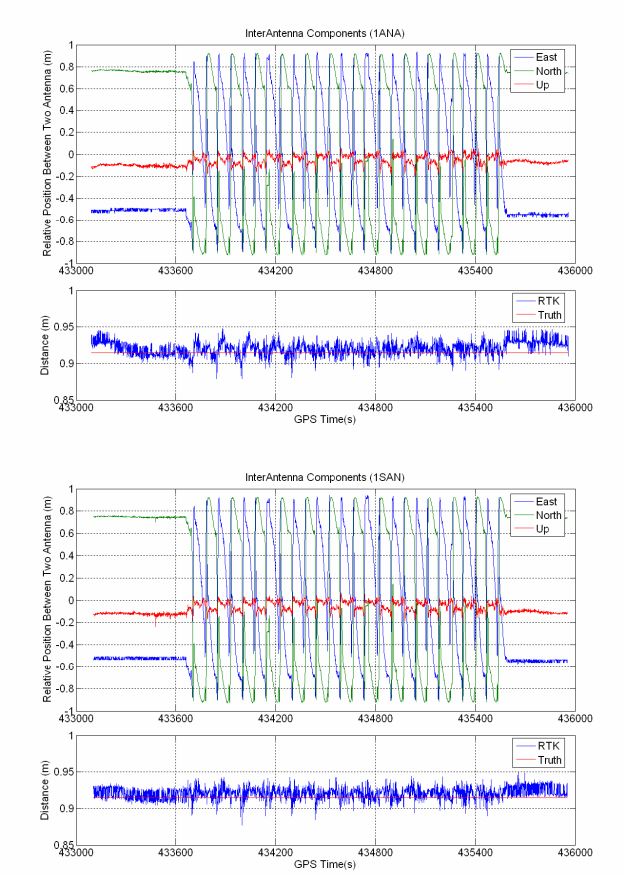

Figure (15) Distance difference between the different antennas

CONCLUSIONS

In this paper, three innovative algorithms have been proposed. First one is to extend functional model to estimate the significant atmospheric residual biases, integration of real time orbit corrections from WADGPS systems. The second is to modify Kalman filter with optimal detection and estimation of cycle slips and code outliers, and partial search and fix strategies embedded in the Kalman filter parameter estimation. Last one is the partial search and fix technique.

Development of the algorithms has been completed including extensive offline testing with recorded data and hosting of the real time version in the target GPS receiver. Both offline and real time results are presented from extensive recorded data runs over baselines ranging up to 75 km. The tests show that the 99.99% fix reliability can be achieved for 10km or less baselines and 99.9% reliability still can be achieved for baselines up to 40km. As the baselines exceed 40km, the reliability decreases to 99.6% at a baseline of 75km. Ambiguity search times are typically one or two 1Hz epochs for short baselines and 1-2s increase per km for over 20km baselines. The new positioning accuracy specifications at 1cm + 0.5ppm in horizontal and 2cm + 1pmm in vertical can be achieved for this newly enhanced RTK engine.

ACKNOWLEDGMENTS

The authors would like to thank Ron Hatch for his useful suggestions and correctness of final paper, Chaochao Wang and Mark Stuebs for collecting and analyzing kinematic test results.

REFERENCES

L. Dai, S. Han & C. Rizos (1999) *A multiple outlier detection algorithm for instantaneous ambiguity resolution for carrier phase-based GNSS positioning.* Int. Symp. on Digital Earth (ISDE), Beijing, P.R. China, 29 November - 2 December, 321-332.

R. Hatch, T. Sharpe, and Y. Yang (2003) *A Simple RAIM and Fault Isolation Scheme*, ION GPS/GNSS 2003, 9-12 September 2003, Portland Oregon.

R. Hatch, T. Sharpe, and Y. Yang (2004) *An Innovative Algorithm for Carrier-Phase Navigation*, ION GPS/GNSS 2004, 9-12 September 2004, Long Beach, California.